



OPEN

The plasminogen protein is associated with high myopia as revealed by the iTRAQ-based proteomic analysis of the aqueous humor

Kai Wen^{1,3}, Xianfeng Shao^{1,3}, Yahong Li¹, Yaoling Li¹, Yongtao Li¹, Qing Wang¹, Ruihong Su¹, Lujie Zhang², Yang Cai¹, Jing Sun¹✉ & Yan Zhang¹✉

To explore the pathogenesis of high myopia (HM) using quantitative proteomics. The aqueous humor of patients with simple nuclear cataract and nuclear cataract complicated with HM (hereinafter referred to as “C” and “HM” groups, respectively) were collected. The isobaric tags for relative and absolute quantitation (iTRAQ)-based liquid chromatography–tandem mass spectrometry (LC–MS/MS) proteomics approach was employed to explore differentially expressed proteins (DEPs). Bioinformatics was used to interpret the proteomic results. Furthermore, the plasminogen (PLG) protein was confirmed by enzyme-linked immunosorbent assay (ELISA) as the candidate biomarker for HM through a receiver operating characteristic curve analysis. The study showed 32 upregulated and 26 downregulated proteins. The gene ontology analysis demonstrated that 58 DEPs corresponded to 325 biological processes, 33 cell components, and 45 molecular functional annotations. The Kyoto Encyclopedia of Genes and Genomes analysis showed that the upregulated DEPs were highly enriched in the coagulation and complement cascades, consistent with the gene set enrichment analysis. Our data suggested that some DEPs might be hallmarks of the development of HM. ELISA confirmed that the PLG expression levels were significantly upregulated in HM. This was a new study investigating alterations in protein levels and affected pathways in HM using iTRAQ-based quantitative proteomics. Our study provided a comprehensive dataset on overall protein changes and shed light on its potential molecular mechanism in human HM.

High myopia (HM), defined as myopia exceeding 6.00 diopters (D) or axis length ≥ 26 mm, significantly increases the risk of pathologic ocular changes¹. A study pointed out that at present, 163 million people are suffering from HM, accounting for 2.7% of the world's total population, and that in the future, HM will show a significant increase in prevalence globally, affecting nearly 1 billion people by 2050². In addition to environmental factors, genetic predisposition seems to play a role in the development of HM. In recent years, the development of new technologies, such as the genome-wide association analysis, has advanced studies on candidate genes in many traditional HM loci, such as MYP1 and MYP2. Several new gene loci, such as MYP20 and MYP21, have been discovered^{3,4}. However, the mechanism of pathological damage in the eyes with HM is unclear.

Proteomics provides a new perspective and method for identifying the pathogenesis of diseases. The proteomic analysis of the aqueous humor in various ocular diseases, including diabetic retinopathy, primary open-angle glaucoma, cataract, and myopia, revealed protein biomarkers of the mechanisms, diagnosis, and novel therapies for the diseases^{5–9}. The aqueous humor is an intraocular fluid that supplies nutrients and removes metabolic wastes from avascular tissues of the eye. It has been used to identify the correlation between altered protein expressions and the prognosis of many eye diseases^{5,8–10}. However, there is no proteomic study on the mechanism of eye damage caused by HM. Proteomics can demonstrate high-throughput quantitative protein

¹Tianjin Key Laboratory of Retinal Functions and Diseases, Tianjin Branch of National Clinical Research Center for Ocular Disease, Eye Institute and School of Optometry, Tianjin Medical University Eye Hospital, No. 251, Fukang Road, Nankai District, Tianjin 300110, China. ²Tianjin Children's Hospital, Tianjin, China. ³These authors contributed equally: Kai Wen and Xianfeng Shao. ✉email: TMUeye@163.com; yanzhang04@tmu.edu.cn

| Samples | Gender | | Ages | | Axial | | Eye | |
|----------|--------|----|--------------|--------------|--------------|--------------|-----|----|
| | C | HM | C | HM | C | HM | C | HM |
| 1 | F | M | 73 | 60 | 23.69 | 29.20 | OD | OS |
| 2 | F | M | 59 | 78 | 23.67 | 29.69 | OD | OS |
| 3 | F | M | 73 | 59 | 23.17 | 29.95 | OS | OD |
| 4 | F | M | 58 | 59 | 25.42 | 29.71 | OS | OS |
| 5 | F | M | 68 | 78 | 22.92 | 29.56 | OS | OS |
| 6 | M | F | 61 | 78 | 22.92 | 29.56 | OS | OS |
| 7 | M | F | 66 | 70 | 23.97 | 26.29 | OS | OD |
| <i>P</i> | | | 0.578 | | <0.01 | | | |
| Mean | | | 65.43 ± 6.29 | 67.71 ± 8.50 | 23.93 ± 0.87 | 28.69 ± 1.61 | | |

Table 1. Patient characteristics. *C* simple nuclear cataract, *HM* nuclear cataract complicated with high myopia, *F* female, *M* male.

| | 113 | 114 | 115 | 116 | 117 | 118 | 119 | 121 |
|------------------|-----|-----|-----|-----|-----|-----|-----|-----|
| iTRAQ 8plex kit1 | QC | C | HM | C | HM | C | HM | C |
| iTRAQ 8plex kit2 | QC | HM | C | HM | C | HM | C | HM |

Table 2. The experimental design of iTRAQ experiments.

expressions, which provide new theoretical bases and solutions for discovering disease mechanisms. The isobaric tags for relative and absolute quantification (iTRAQ) technology developed by AB SCIEX, USA is an accurate quantitative technique for in vitro isotopic labeling. It uses up to eight isotope reagents to label the N-terminal or lysine side chain of peptides. A high-resolution mass spectrometer can simultaneously analyze the protein expression of these eight samples. It has been a promising quantitative technique in proteomics in recent years.

In the present study, we performed the iTRAQ-based quantitative proteomic analysis of the aqueous humor of patients with nuclear cataract complicated with HM and simple nuclear cataract to identify functional proteins associated with the pathogenesis of HM. Additionally, we performed enzyme-linked immunosorbent assay (ELISA) to confirm the iTRAQ results. Our findings are likely to enhance our understanding of the mechanisms of HM in humans.

Materials and methods

Aqueous humor samples. In this prospective study, patients with simple nuclear cataract and nuclear cataract complicated with HM (hereinafter referred to as “C” and “HM” groups, respectively) who first visited the Tianjin Medical University Eye Hospital (Tianjin, China) were enrolled, and their aqueous humor samples were collected during cataract surgery. Inclusion criteria were nuclear cataract and an axis length ≥ 26 mm. Exclusion criteria were other eye and systemic diseases, such as hypertension, diabetes, coronary heart disease, and autoimmune disease. Fourteen aqueous humor samples of eleven patients, including seven samples from each group, were selected in the study. Table 1 shows patient characteristics. Informed consent was obtained from all participants of this study. The collection and preparation of the samples are performed by the same skilled surgeon as follows. 2 eye drops of oxybuprocaine hydrochloride 0.4% (Beinuoxi, Santen Pharmaceutical Co., Ltd, Osaka, Japan) were applied to the eye before rinsing twice with 0.5% povidine iodine (Anerdian, LikangDisinfection Co., Ltd, Shanghai, China). After that, the conjunctival sac was irrigated with a balanced salt solution before the aqueous humor sample collection. To avoid blood and other ocular surface contaminants, the sample was collected using a 1 mL tuberculin syringe with a 30 gauge needle at the corneal limbus prior to any other entry into the eye under the surgical microscope. Then, all samples were collected into a cryopreservation tube and stored at -80 °C until use. This study was approved by the Human Research Ethics Committee of the Tianjin Medical University Eye Hospital and adhered to the tenets of the Declaration of Helsinki.

Sample preparation. We lysed 50 μ L aqueous humor with 350 μ L 8 M urea buffer (8 M urea [Sigma], 100 mM triethylammonium bicarbonate [TEAB; Sigma], 1 \times protease inhibitor [Roche]) at room temperature for 5 min. The lysis products were sonicated on ice and centrifuged at 16,000 \times g for 10 min at 15 °C. After removing precipitates, the protein concentration was measured by bicinchoninic acid kits (Solabio). For each sample, 100 μ g total protein was transferred into a new 1.5-mL tube, and 10 mM DL-dithiothreitol (Sigma) was added and incubated at 37 °C for 1 h. Subsequently, 40 mM iodoacetamide (Sigma) was added and incubated in dark for 1 h at room temperature. For balance, 400 μ L 100 mM TEAB was added to a 10 kDa filter (Sartorius). The sample was transferred onto the filter and centrifuged at 14,000 \times g for 20 min at 4 °C. The sample was washed thrice with 400 μ L of 100 mM TEAB and collected using a new tube with 100 μ L of 100 mM TEAB. For digestion, 2 μ g sequencing grade modified trypsin was used for digestion at 37 °C for 12–16 h. The resulting peptides were dried with SpeedVac (Thermo Fisher, SPD1010). iTRAQ 8-plex kits were used to label the peptides by following the manufacturer’s protocols (Table 2). To normalize protein expression, the quality control sample,

pooled from an equal amount of aqueous humor of 14 patients, was labeled with mass tag 113. Small high pH reversed-phase peptide fractionation columns were used to fractionate samples with gradually increasing acetonitrile concentrations (6%, 9%, 12%, 15%, 18%, 21%, 25%, 30%, and 35%). The nine fractions were combined into six (6% + 25%, 9% + 30%, 12% + 35%, 15%, 18%, and 21%). Peptides were dried and resuspended with 0.1% formic acid.

LC–MS/MS analysis. Samples were analyzed with the TripleTOF 6600 mass spectrometer (AB SCIEX, USA) coupled with the ekspert nano-LC 415 nanoflow LC system (AB SCIEX, USA). Fractionated peptides were loaded onto an in-house made trap (100 $\mu\text{m} \times 2$ cm; particle size, 3 μm ; SunChrom, USA) with mobile phase A (v/v/v, 2% acetonitrile, 0.1% formic acid, and 97.9% water) and separated with a linear gradient of mobile phase B (v/v/v, 0.1% formic acid, 97.9% acetonitrile, and 2% water) on the analytical column (150 $\mu\text{m} \times 15$ cm; particle size, 1.9 μm ; SunChrom, USA). The effective elution gradient was 5–35% for 1.5 h at a flow rate of 600 nL/min. The accumulation times for time-of-flight MS and product ions were 0.25 and 0.04 s, respectively. The mass ranged from 300 to 1500 m/z. The charge state ranged from +2 to +5, and mass tolerance was less than 50 ppm. We monitored 60 ions/cycle, and the ion exclusion time was 16 s. The fragmentation energy was adjusted using iTRAQ reagents, and a high sensitivity mode was used for scanning.

Protein identification and quantification. For each iTRAQ set, raw files from eight fractions were combined to search a human database (Swiss human database, released in March 2019, comprising 20,425 entries) with MaxQuant software version 1.6.4.0. Dynamic modifications included N-acetylation, oxidation of methionine, and cysteine carbamidomethylation as the fixed modification. All reporter ions were applied for quantification. The false discovery rate (FDR) was set at 1% for both peptide spectrum matches and proteins. At least two peptides per protein were chosen for quantification. The mass tolerance was 0.1 Da for precursor ions and 50 ppm for fragment ions.

Statistical and bioinformatic analyses. Data were normalized with quality control between two iTRAQ sets, and median normalization was applied to adjust the error among samples. Student's *t*-test was applied to calculate *p*-values. Screened proteins with a *p* value < 0.05 and fold change > 1.5 were considered to be significantly expressed. The gene ontology (GO) and KEGG pathway^{11,12} enrichment analysis was processed through cluster Profiler, an R package. The adjusted *p*- and *q*-values were both < 0.05. Protein–protein interactions (PPIs) were analyzed with a web tool called STRING, version 11.0, and visualized with Cytoscape software version 3.7.0. Proteins were classified according to their annotated functions. The gene set enrichment analysis (GSEA) was executed with GSEA software version 3.0 (FDR < 0.25, normalized *p* value < 0.05). The principal component analysis was conducted with the stats package and visualized with the factoextra R package.

ELISA and receiver operating characteristic (ROC) curve analysis. The target protein plasminogen (PLG) was chosen for verification of differential expressions using ELISA. The Human Plasminogen ELISA kit (Elabscience Biotechnology Co., Ltd., E-EL-H2102c) was used. ELISA assays were performed according to the manufacturer's protocols, and samples (HM group, 14 samples; C group, 10 samples) were run in duplicate. The absorbances of the standards and samples were determined by spectrophotometry at 450 nm with a microplate reader. Statistical analyses were performed with GraphPad Prism version 6.0. Student's *t*-test was applied for comparisons of quantitative data, and the ROC curve analysis with GraphPad Prism version 6.0 was performed to evaluate the sensitivity and specificity of the protein PLG.

Results

Quantitative proteomic analysis. Aqueous humor proteins that showed differential accumulation between C and HM groups were identified and analyzed with LC–MS/MS. In the proteomic analysis, a total of 211 unique corresponding proteins were quantified. Among proteins showing significant changes (*p* < 0.05) in abundance, we used proteins with values of an abundance fold change > 1.5 to identify those with a significant difference in abundance between the C and HM groups. Figure 1 shows the experimental design of the whole study.

The study showed 58 differentially expressed proteins (DEPs), including 32 upregulated and 26 downregulated proteins (Table 3). The hierarchical cluster analysis showed that the expression pattern of DEPs differed between the two groups (Fig. 2A). Consistently, the results of the principal component analysis and volcano plot showed that DEPs were distributed in two different quadrants (Fig. 2B,C). Among these proteins, the five most upregulated proteins were P0COL5 (complement), P00747 (plasminogen), Q86YA3 (protein ZGRF1), Q14515 (high endothelial venule protein), and A0A075B6K5 (immunoglobulin lambda variable 3–9), and five most downregulated proteins were P01780 (immunoglobulin heavy variable 3–7), P23142 (fibulin-1), A0A0A0MS15 (immunoglobulin heavy variable 3–49), P31025 (lipocalin-1), and P02750 (rho-GTPase-activating protein LRG1). The significant difference in abundance indicated the complex changes of proteome in HM under the refractive state.

Bioinformatic analysis of DEPs. *Data quality control.* Figure 3A shows the Pearson correlation coefficients of the samples. The correlation coefficients in control and HM groups were above 0.96 and 0.87, respectively, indicating high reproducibility of the data.

GO analysis. To evaluate the major biological processes that can be perturbed by HM, the GO enrichment analysis was performed on DEPs. The results showed that 58 DEPs were involved in 403 functional annotations.

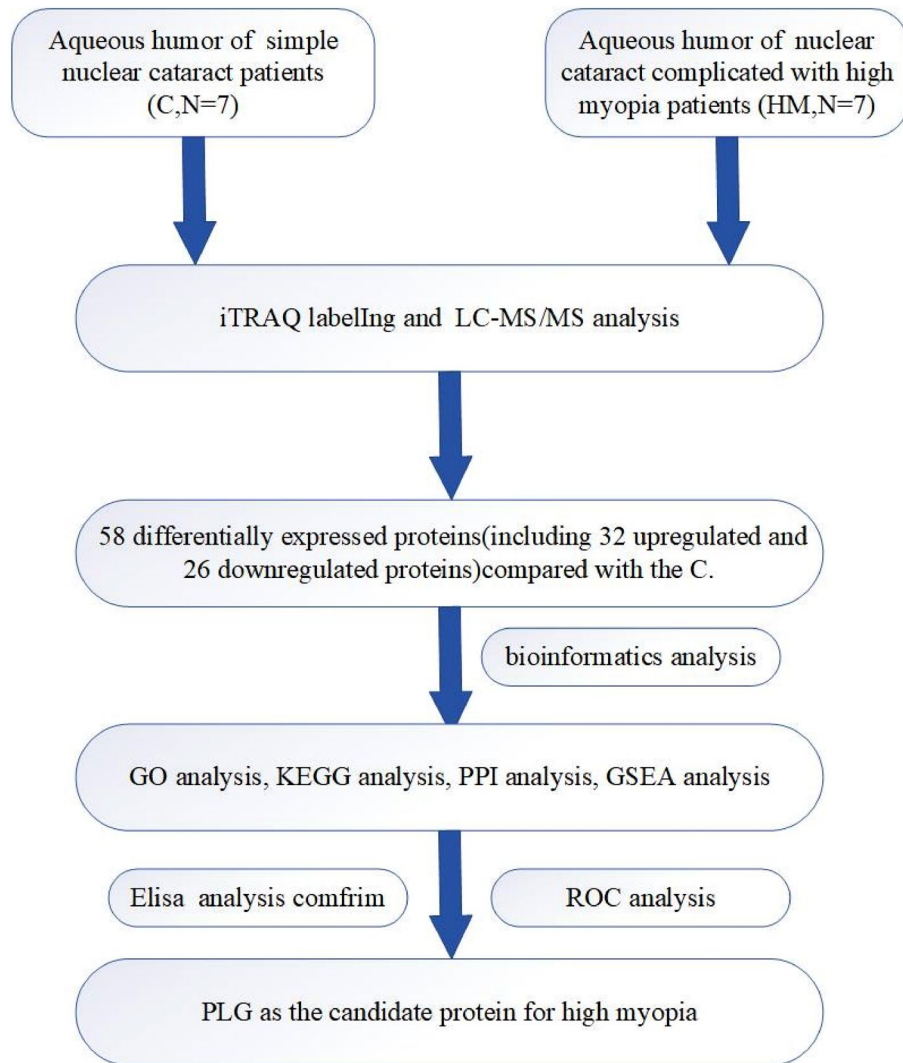


Figure 1. The experimental plan of the present study. iTRAQ was applied to identify the differentially expressed proteins in C and HM. PLG was candidate protein for pathogenesis of high myopia.

Figures 3B (DEPs involved) and C (downregulated DEPs involved) present the enrichment analysis results. The most significant annotation functions were the acute inflammatory response, platelet degranulation, and protein activation cascade for upregulated proteins and protein activation cascade, humoral immune response, and complement activation for downregulated proteins.

KEGG analysis. To analyze the main biochemical processes and associated pathophysiological pathways affected by HM, a KEGG pathway^{11,12}-based enrichment analysis was conducted to determine the DEPs in the aqueous humor. The affected pathways upregulated the proteins involved in the complement and coagulation cascades and cholesterol metabolism (Fig. 4A) and downregulated the proteins involved in glycolysis/gluconeogenesis, biosynthesis of amino acids, and HIF-1 signaling pathway (Fig. 4B). A total of eight DEPs were confirmed as key signal molecules of these pathways, including C4B (complement), PLG (plasminogen), C9 (complement component), F2 (thrombin), KNG1 (kininogen-1), CF1 (cleavage stimulation factor subunit 2), SERPINA1 (alpha-1-antitrypsin), and C4A (complement). GO showed that DEPs were mainly associated with inflammation and humoral immunity, and the major proteins involved (C4B, PLG, C9, F2, CFI, SERPINA1, and C4A) coincided with the complement coagulation cascade, implying that DEPs may participate in the process of eye damage caused by HM through the immune process involved in the complement system.

Moreover, we performed GSEA ($p < 0.05$, FDR < 0.25) on DEPs and found that the two classical signaling pathways, the complement coagulation cascade and extracellular matrix regulator, were enriched and upregulated (Fig. 5A–C). Consistent with the previous KEGG results, the major enriched proteins were C4B, PLG, KNG1, C9, F2, CFI, SERPINA1, and C4A. The results of Riddell Nina on HM chicken model showed that complement coagulation cascade and extracellular matrix pathway were overexpressed in HM¹³. It further suggests that the above proteins may be the key factors of pathogenicity.

| Accession | Gene symbol | Sequence length | Description | p value |
|-------------------------------|-------------|-----------------|---|-------------|
| Downregulated proteins | | | | |
| P01780 | IGHV3-7 | 117 | Immunoglobulin heavy variable 3-7 | 5.89E-07 |
| P23142 | FBLN1 | 703 | Fibulin-1 | 1.03089E-04 |
| A0A0A0MS15 | IGHV3-49 | 119 | Immunoglobulin heavy variable 3-49 | 4.56645E-06 |
| P31025 | LCN1 | 176 | Lipocalin-1 | 0.0324 |
| P02750 | LRG1 | 347 | Leucine-rich alpha-2-glycoprotein | 0.0039 |
| P35555 | FBN1 | 2871 | Fibrillin-1 | 0.0005 |
| O14773 | TPP1 | 563 | Tripeptidyl-peptidase 1 | 0.0002 |
| O15537 | RS1 | 224 | Retinoschisin | 0.0002 |
| P43251 | BTD | 543 | Biotinidase | 1.18505E-05 |
| Q08380 | LGALS3BP | 585 | Galectin-3-binding protein | 5.27E-06 |
| P04433 | IGKV3-11 | 115 | Immunoglobulin kappa variable 3-11 | 3.09E-06 |
| P06733 | ENO1 | 434 | Alpha-enolase | 2.55032E-05 |
| P07602 | PSAP | 524 | Prosaposin | 0.0007 |
| P01023 | A2M | 1474 | Alpha-2-macroglobulin | 0.0001 |
| Q06481 | APLP2 | 763 | Amyloid-like protein 2 | 0.0060 |
| P04196 | HRG | 525 | Histidine-rich glycoprotein | 0.0020 |
| P51884 | LUM | 338 | Lumican | 0.0029 |
| P36222 | CHI3L1 | 383 | Chitinase-3-like protein 1 | 0.0385 |
| P04406 | GAPDH | 335 | Glyceraldehyde-3-phosphate dehydrogenase | 0.0364 |
| P01859 | IGHG2 | 326 | Immunoglobulin heavy constant gamma 2 | 0.0031 |
| P16870 | CPE | 476 | Carboxypeptidase E | 0.0119 |
| P0DP03 | IGHV3-30-5 | 117 | Immunoglobulin heavy variable 3-30-5 | 0.0178 |
| P10745 | RBP3 | 1247 | Retinol-binding protein 3 | 0.0010 |
| P01825 | IGHV4-59 | 116 | Immunoglobulin heavy variable 4-59 | 0.0204 |
| P02656 | APOC3 | 99 | Apolipoprotein C-III | 0.0263 |
| P08185 | SERPINA6 | 405 | Corticosteroid-binding globulin | 0.0318 |
| Upregulated proteins | | | | |
| P02790 | HPX | 462 | Hemopexin | 0.0002 |
| P05090 | APOD | 189 | Apolipoprotein D | 0.0358 |
| P02749 | APOH | 345 | Beta-2-glycoprotein 1 | 0.0236 |
| P00450 | CP | 1065 | Ceruloplasmin | 0.0005 |
| P43652 | AFM | 599 | Afamin | 0.0074 |
| Q8N945 | PRELID2 | 189 | PRELI domain-containing protein 2 | 0.0485 |
| P0COL4 | C4A | 1744 | Complement C4-A | 0.0004 |
| P00441 | SOD1 | 154 | Superoxide dismutase [Cu-Zn] | 0.0427 |
| P02652 | APOA2 | 100 | Apolipoprotein A-II | 0.0319 |
| P01834 | IGKC | 107 | Immunoglobulin kappa constant | 0.0002 |
| P01009 | SERPINA1 | 418 | Alpha-1-antitrypsin | 0.0065 |
| Q15582 | TGFBI | 683 | Transforming growth factor-beta-induced protein ig-h3 | 0.0086 |
| P02753 | RBP4 | 201 | Retinol-binding protein 4 | 0.0069 |
| P05156 | CFI | 583 | P05156 | 0.0001 |
| P01042 | KNG1 | 644 | Kininogen-1 | 0.0003 |
| P19652 | ORM2 | 201 | Alpha-1-acid glycoprotein 2 | 0.0012 |
| P02760 | AMBP | 352 | Protein AMBP | 0.0003 |
| Q9BU40 | CHRD1 | 456 | Chordin-like protein 1 | 0.0099 |
| P55083 | MFAP4 | 255 | Microfibril-associated glycoprotein 4 | 0.0186 |
| P00734 | F2 | 622 | Prothrombin | 0.0008 |
| P02647 | APOA1 | 267 | Apolipoprotein A-I | 0.0019 |
| Q6EMK4 | VASN | 673 | Vasorin | 8.22652E-06 |
| P02748 | C9 | 559 | Complement component C9 | 0.0002 |
| P06727 | APOA4 | 396 | Apolipoprotein A-IV | 3.60425E-05 |
| P01011 | SERPINA3 | 423 | Alpha-1-antichymotrypsin | 2.15865E-05 |
| P01019 | AGT | 485 | Angiotensinogen | 3.89348E-05 |
| Q86UP8 | GTF2IRD2 | 994 | General transcription factor II-I repeat domain-containing protein 2A | 0.0017 |
| A0A075B6K5 | IGLV3-9 | 115 | Immunoglobulin lambda variable 3-9 | 7.01549E-05 |
| Continued | | | | |

| Accession | Gene symbol | Sequence length | Description | <i>p</i> value |
|-----------|-------------|-----------------|----------------------|----------------|
| Q14515 | SPARCL1 | 664 | SPARC-like protein 1 | 0.017036259 |
| Q86YA3 | ZGRF1 | 2104 | Protein ZGRF1 | 0.0006 |
| P00747 | PLG | 810 | Plasminogen | 1.43342E-05 |
| P0C0L5 | C4B | 1744 | Complement C4-B | 4.38E-08 |

Table 3. Quantitative proteomic analysis of 58 differentially expressed proteins, including 32 upregulated and 26 downregulated proteins.

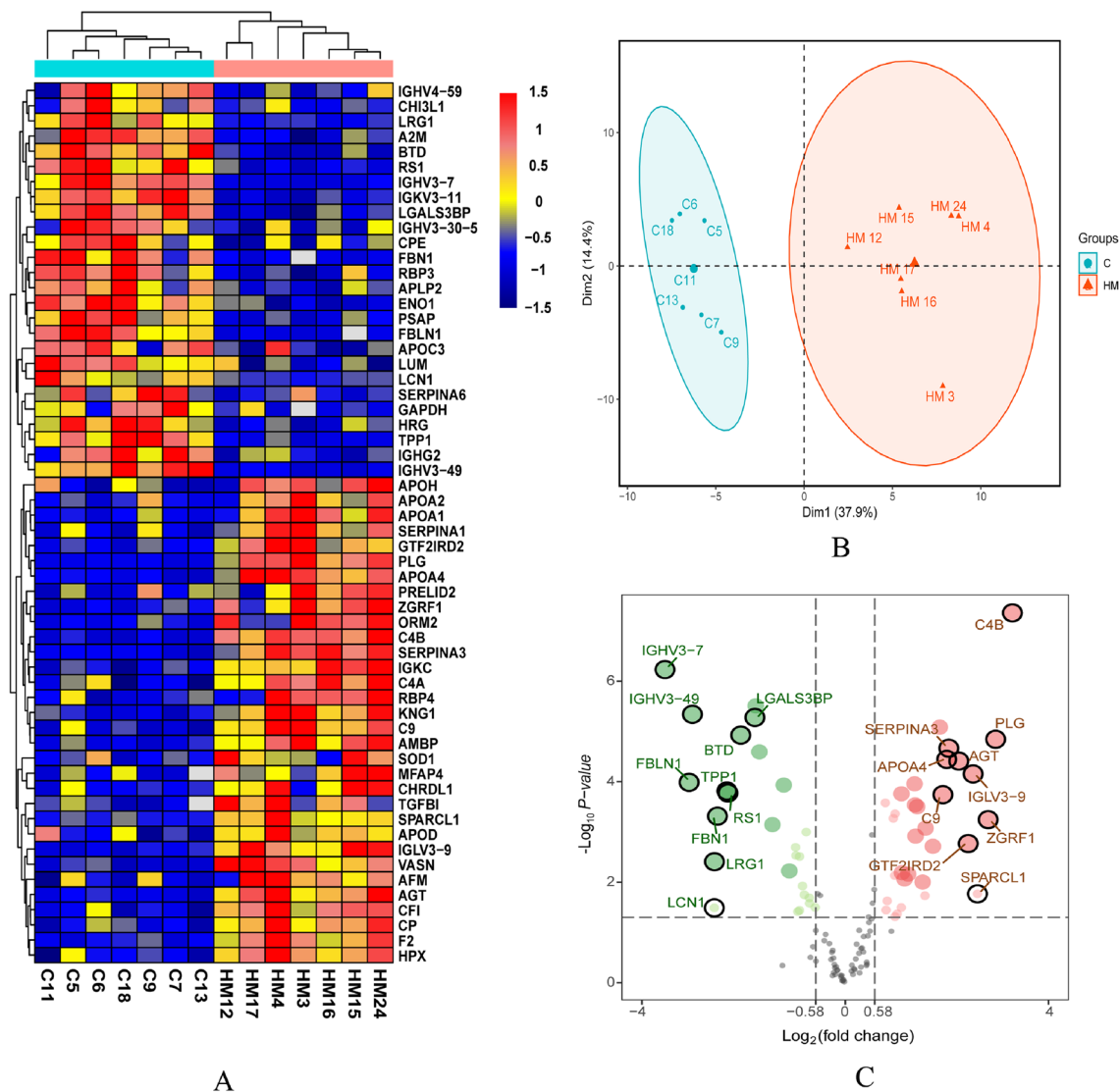


Figure 2. (A) Hierarchical cluster analysis of the differentially expressed proteins (Columns represent samples, rows represent proteins, and the shorter the distance of cluster branches represents the higher the similarity of proteins). Red represents up-regulated proteins and blue represents down-regulated proteins. (B) The result of principal component analysis (PCA), indicating that there were significant differences in protein expression between the C and HM. (C) Differential protein volcano plot showed that these were distributed in two different quadrants (The logarithm of the fold change of each quantifiable protein was taken as base 2, and the negative logarithm of the *P* value was taken as base 10). Horizontal axis represents the fold change (\log_2 value) of the differential protein, and vertical axis represents the *P* value ($-\log_{10}$ value). Gray dots represent proteins with insignificant differences, red dots represent up-regulated proteins, and blue dots represent down-regulated proteins. The top10 protein was selected to display.

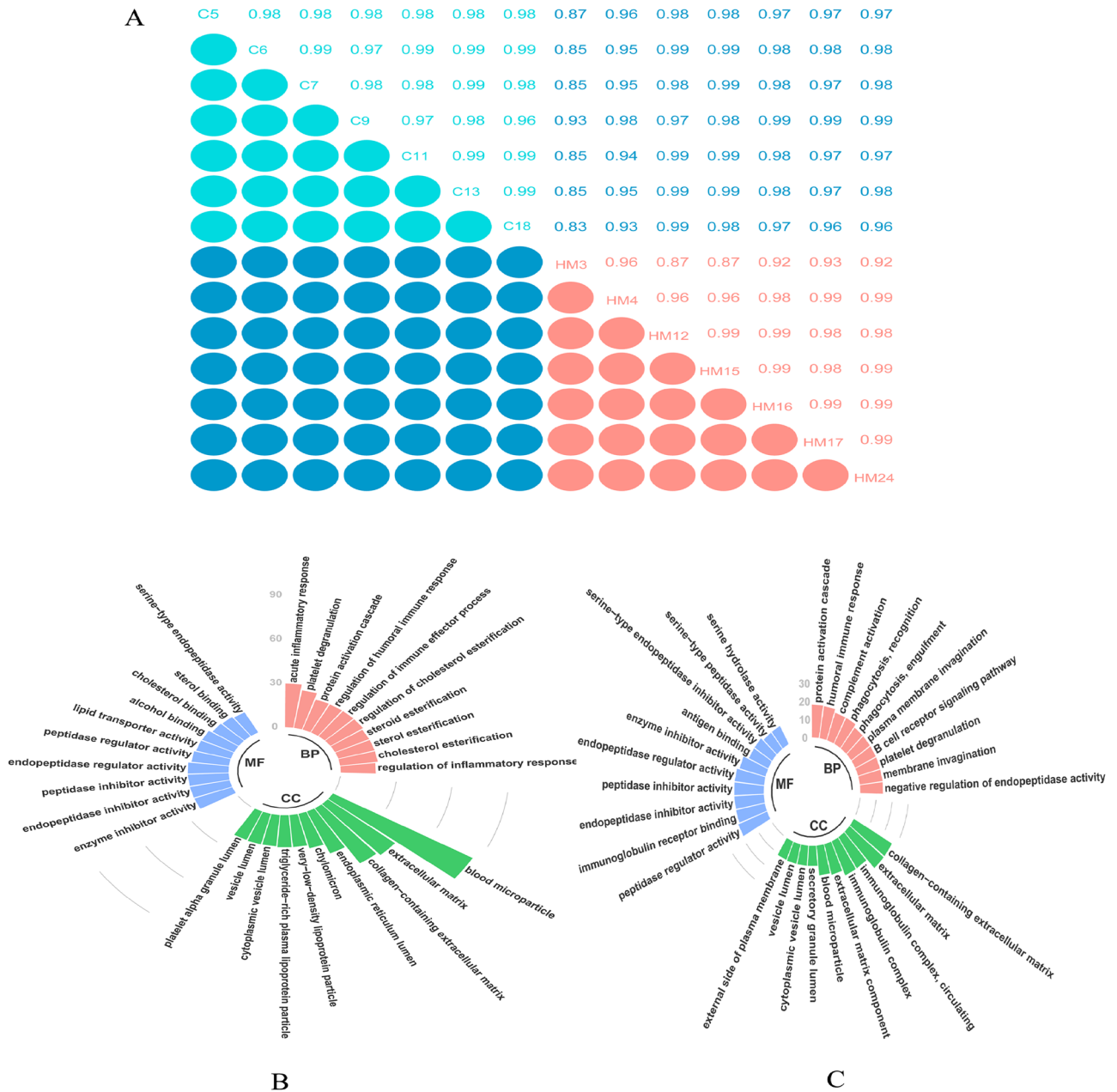
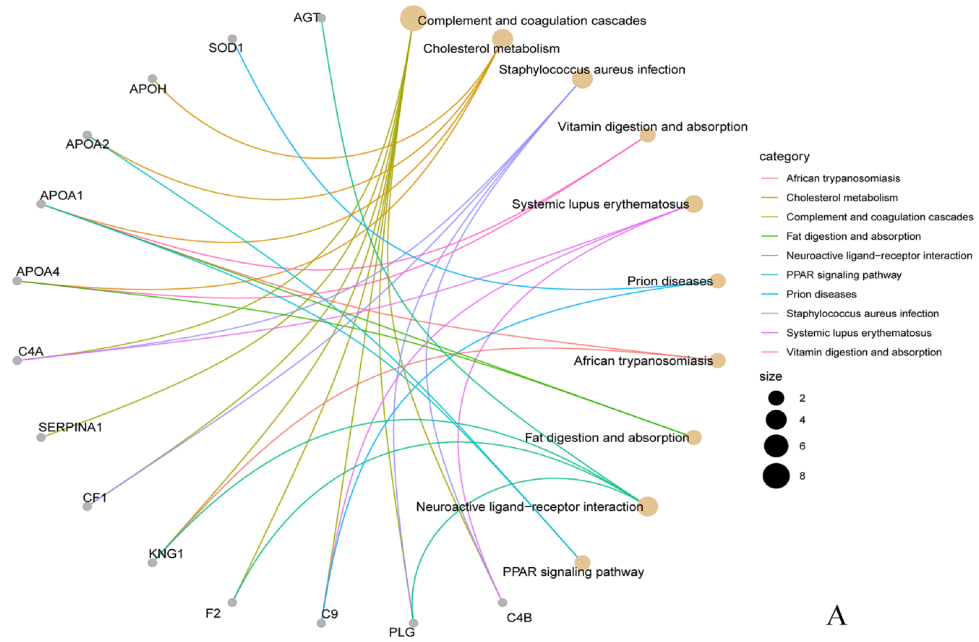


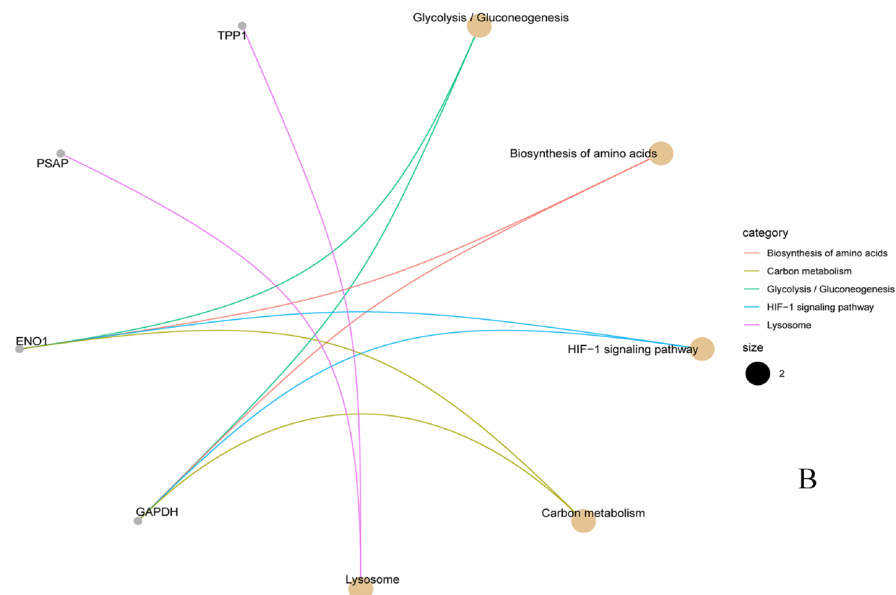
Figure 3. (A) Pearson correlation coefficient between samples showed overall data quality. (B) and (C) Gene Ontology (GO) classification of the upregulated differentially expressed proteins and downregulated differentially expressed proteins, respectively. Proteins were classified into three main categories: biological process, cellular component, and molecular.

PPI analysis. In order to further decipher the potential function of these DEPs, PPIs were analyzed with the STRING database and classified according to DEP functions (information from GO, UniProt, and NCBI). These interacting proteins were divided into six categories, mainly involved in the complement coagulation cascade, enzyme inhibitor activity, lipid metabolism, cell adhesion, and immune response. Figure 6A presents the results.

Target protein. Pearson's correlation analysis of the proteins involved in the GSEA complement coagulation cascade revealed that proteins had a strong correlation in expression (Fig. 6B). Previous studies suggested that collagens I and XVIII played an important role in the pathogenesis of posterior scleral staphyloma caused by HM^{14,15}. In the interactions among collagen I, collagen XVIII, and proteins involved in the complement coagulation cascade, SERPINA1, PLG, KNG1, F2, C4A were proteins with high interaction degree (Fig. 6C). Among the five hub DEPs, PLG had the largest expression fold change (7.78), which was equal to the sum of SERPINA1 (2.17), KNG1 (2.59), and F2 (2.99). And PLG is a member of fibrinolytic system, which plays a role in extracellular matrix remodeling and coagulation cascade (Fig. 5C). Therefore, PLG may be the most hub one among them.



A



B

Figure 4. (A) and (B) Kyoto Encyclopedia of Genes and Genomes (KEGG) enrichment analysis of the upregulated differentially expressed proteins and downregulated differentially expressed proteins, respectively (Select the top 10 by the value of p.adjust).

Validation with ELISA. We used the ELISA kit to verify the PLG protein expression in the aqueous humor of patients with HM. Figure 7A shows the iTRAQ quantification in the MS/MS spectrum. The expression levels of PLG were significantly upregulated in HM (Fig. 7B), which showed the same trend of change as the proteomic results.

ROC curve analysis. The areas under the ROC curves were calculated as measures of the specificity and sensitivity of the confirmed protein (Fig. 7C). The accuracy of the area under the ROC curve was assessed as follows: 0.9–1 = excellent; 0.8–0.9 = good; 0.7–0.8 = fair; and < 0.7 = not useful. The ROC analysis identified that PLG was informative (AUC: 0.8750, 95% confidence interval: 0.7280–1.022).

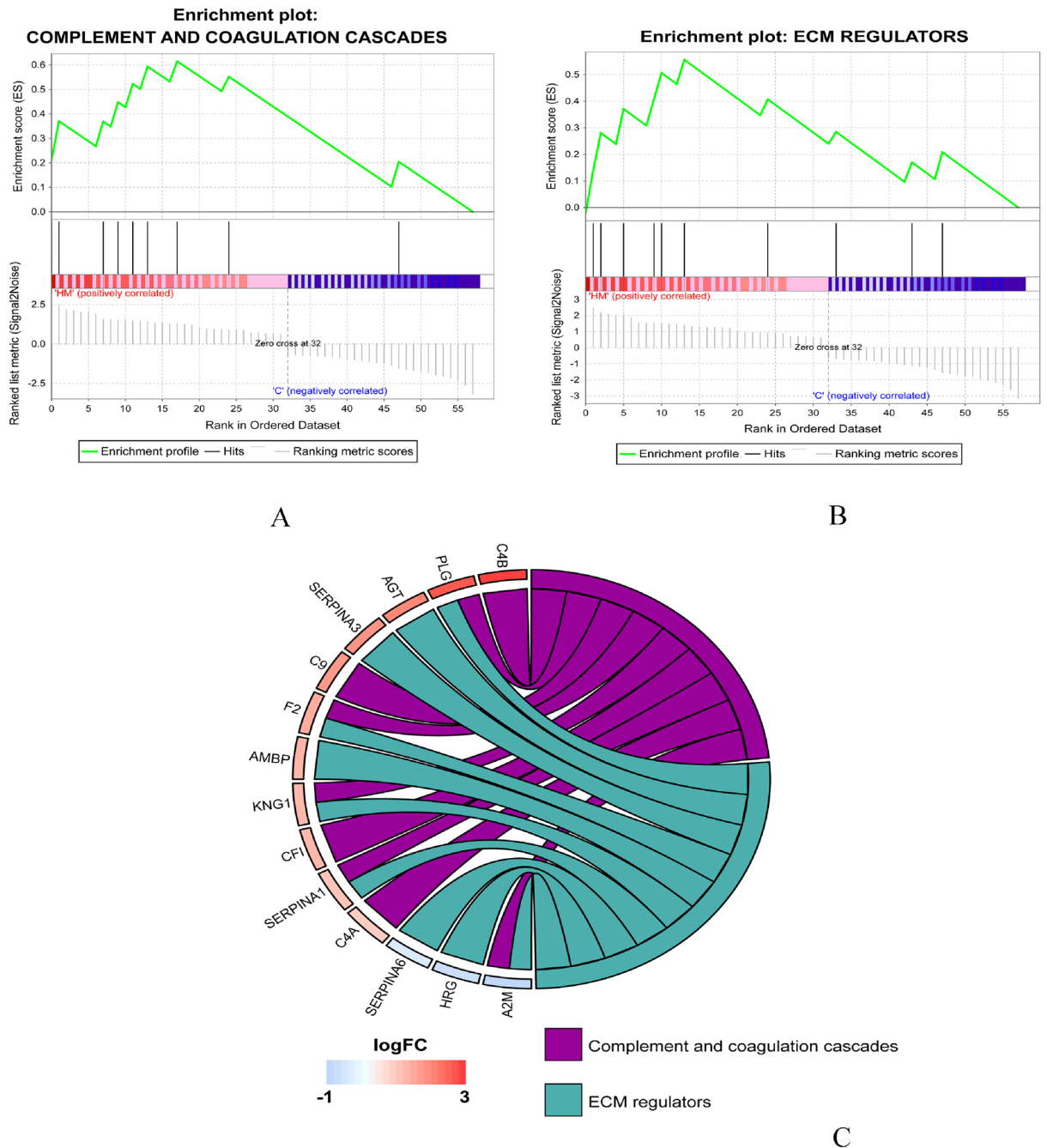


Figure 5. Gene set enrichment analysis showed that the two classical signaling pathways of complement coagulation cascade (A and C) and extracellular matrix regulator (B and C), were enriched and upregulated.

Discussion

The development of HM is associated with changes in the collagen fibers of the sclera, as demonstrated in both human and animal models^{9,14}. Studies have identified numerous proteins that are involved^{9,16,17}. However, to date, most insights regarding HM have come from studies on animal models, which typically focused on the retina, choroid, and sclera⁹. Although changes in protein levels of the aqueous humor in myopic eyes have been extensively studied, few studies have focused on HM. Therefore, the aim of this study was to investigate the changes in aqueous humor protein levels in HM. The results of proteomics might offer new insights to elucidate the mechanism of HM and identify new potential targets for the treatment.

In this study, a total of 211 proteins were identified. The iTRAQ technique revealed 58 DEPs in the aqueous humor of patients with HM, which indicated that the protein expression in the aqueous humor changes in HM. However, the origin and causal relationship with those proteins are unclear. In the study investigating the proteome of the aqueous humor in patients with HM versus controls using iTRAQ-based quantitative proteomics by Xiang M and colleagues, they compared proteins in the aqueous humor of 12 patients undergoing cataract

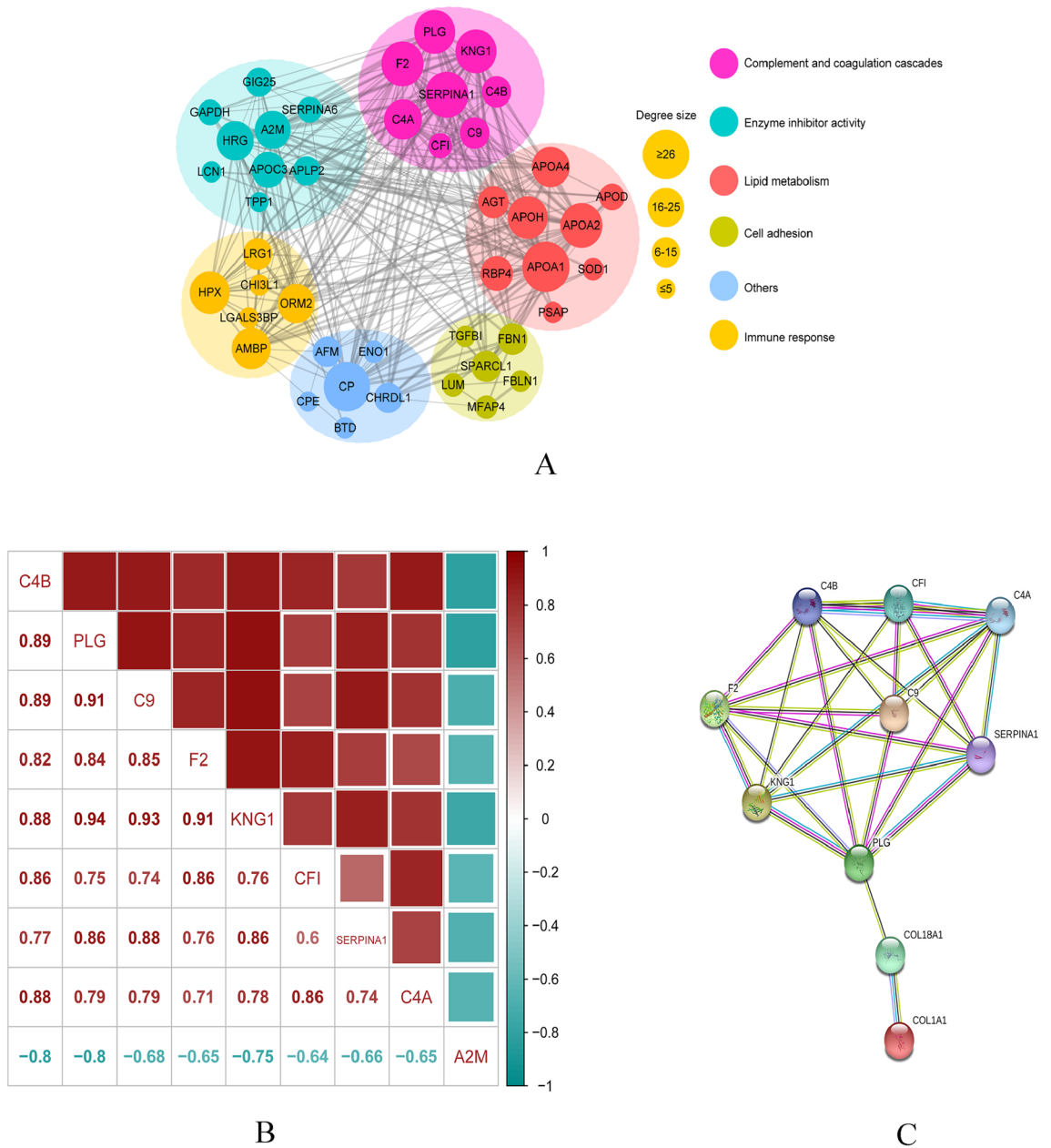


Figure 6. (A) Protein–protein interactions of differentially expressed proteins. (B) Pearson correlation analysis of the proteins involved in the GSEA complement coagulation cascade. (C) Interaction between collagen I, collagen XVIII and the proteins involved in the complement coagulation cascade.

surgery (6 patients with HM, 6 controls) and found 445 proteins including 146 DEPs¹⁸, with no mention of PLG among the significant proteins probably because of sample differences. Duan et al. characterized the aqueous humor of five patients with HM and five age-matched patients with cataract without HM undergoing routine senile cataract surgery and identified that a total of six spots were significantly increased in the two-dimensional gel analysis in HM, with the proteins being albumin, transthyretin, and a vitamin D-binding protein⁹. Transthyretin and the vitamin D-binding protein were included in the 211 proteins we identified but not in the 58 DEPs. This may be caused by differences in protein identification techniques.

The upregulated DEPs were highly concentrated in the coagulation and complement cascade (GSEA and KEGG analysis). A meta-analysis of transcriptome datasets in chick myopia and hyperopia models provided the evidence for involvement of the complement pathway in hyperopia¹³. Some studies showed that the complement system might promote extracellular matrix (ECM) remodeling in the sclera^{13,19}.

PLG can be activated by the tissue or urokinase-type plasminogen activator as active plasmin. Plasmin degrades fibrin and converts potential matrix metalloproteinases (pro-MMPs) into active MMPs, which can destroy the ECM²⁰. Moreover, plasmin plays an important role in many physiological and pathological processes which may be involved in the pathogenesis of high myopia, such as tissue remodeling, angiogenesis^{21–24}.

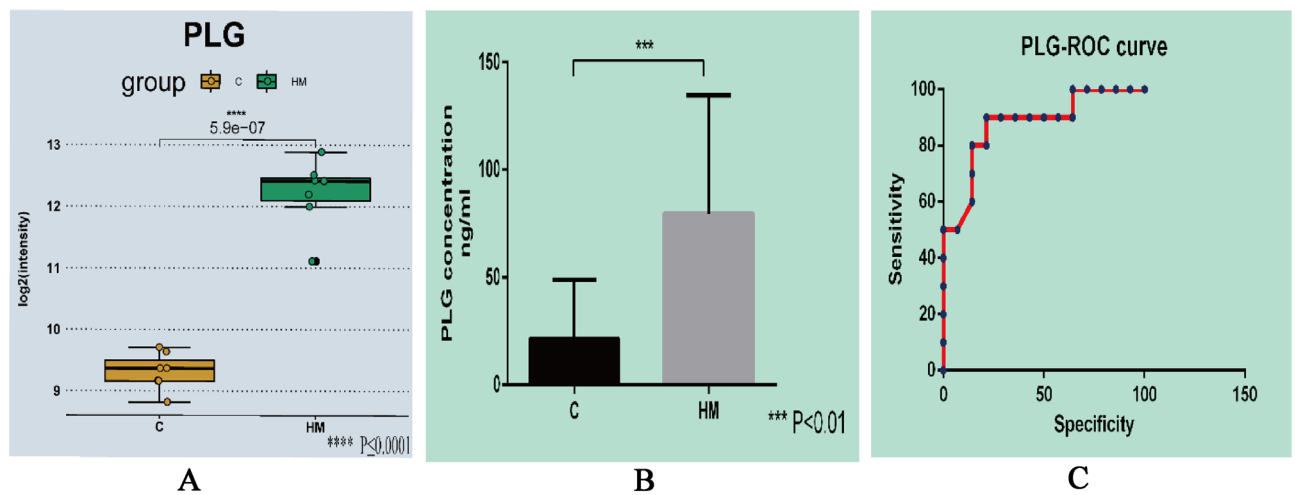


Figure 7. (A) A representative MS/MS spectrum indicated important peptide segments for PLG. (B) Result of ELISA showed the expression levels of PLG were significantly up-regulated in HM compared to C. (C) ROC curve analysis for the specificity and sensitivity of PLG.

Additionally, some studies have shown that plasmin is closely related to inflammation, autoimmunity, tumor formation, and neurodegeneration^{25–27}. Thus, PLG is a multifunctional factor associated with the pathogenesis of HM that warrants further investigations.

Posterior scleral staphyloma is a basic lesion in a series of interrelated degenerative changes in HM and significantly associated with macular holes, retinal detachment, and myopic foveoschisis; therefore, it is recognized as a hallmark of HM²⁸. Previous studies pointed out that the overall scleral thinning observed in highly myopic human eyes were associated with a reduction in size of the individual collagen fibrils with a preponderance of unusually small diameter fibrils averaging below 60–70 nm²⁹. After 12 days of experimental myopia in the tree shrew (equivalent to 12–14 D myopia), the thickness of the posterior sclera had been reduced by 20% and showed a slow, progressive thinning subsequently. Simultaneously, the dry weights of the sclera and the posterior sclera were reduced by 7% and 17%, respectively²⁹. These ultramicroscopic alterations in the sclera of patients with HM suggested that the disorder of the scleral collagen fibrils may be due to the decreased synthesis or increased accentuated breakdown. The overexpression of the PLG protein in HM activates it outside the blood vessels, dissolves the fibers, and makes the sclera thinner, which accelerates the occurrence of posterior scleral staphyloma. According to the website of UniProt (<https://www.uniprot.org/>), KNG1 plays a role in increasing vascular permeability. Therefore, the upregulated KNG1 can damage the blood–retina barrier and increase vascular permeability by regulating the tight junction with the vascular endothelium, which in turn causes inflammatory mediators to enter the aqueous or vitreous humor. Furthermore, the enriched ECM regulatory factor signaling pathway indicates that the activated PLG may reduce scleral hardness by affecting the composition of the scleral connective tissue. Additionally, the classical signaling pathways of the ECM regulator suggest that excessive activation of PLG may reduce the scleral stiffness by affecting the components of scleral connective tissue. The composition of the scleral ECM is the key to maintain its inherent stiffness, strength, and elasticity.

Apart from its potential role in the mechanism of posterior scleral staphyloma caused by HM, PLG plays a role in the pathogenesis of other complications. First, glaucomatous optic neuropathy (GON) is a common cause of irreversible vision loss worldwide. Several hospital- and population-based investigations showed that the prevalence of GON was higher in highly myopic eyes compared to emmetropic eyes^{30–36}. Enlargement of the optic disc, including the stretching and thinning of the sieve plate, may be a factor causing susceptibility to GON³⁷. Therefore, we speculated that fibrinolysis induced by PLG activation may be the main factor of optic disc stretching and cribriform plate thinning in HM, which may also be the reason why patients with HM are prone to normal-tension glaucoma^{38,39}. Additionally, liquefaction of the vitreous humor begins at a relatively young age in patients with HM^{40,41}, which may directly relate to PLG activation. Harocopos and Filas et al. suggested that loss of the vitreous gel with aging increases the risk of nuclear cataracts^{42,43}, which are strongly associated with HM^{44,45}. Therefore, the activation of PLG may be the cause of patients with HM suffering from nuclear cataracts.

Our study had some limitations. First, the sample size was relatively small because of the stringent patient recruitment criteria. Second, we have not conducted further animal and cellular studies on the role of PLG in the pathogenesis of posterior scleral staphyloma. However, the proteomic results were verified using an independent cohort with ELISA (supplementary table).

Received: 18 January 2021; Accepted: 9 April 2021

Published online: 22 April 2021

References

- Wong, T. Y., Ferreira, A., Hughes, R., Carter, G. & Mitchell, P. Epidemiology and disease burden of pathologic myopia and myopic choroidal neovascularization: an evidence-based systematic review. *Am. J. Ophthalmol.* **157**, 9–25e12. <https://doi.org/10.1016/j.ajo.2013.08.010> (2014).
- Holden, B. A. *et al.* Global prevalence of myopia and high myopia and temporal trends from 2000 through 2050. *Ophthalmology* **123**, 1036–1042. <https://doi.org/10.1016/j.ophtha.2016.01.006> (2016).
- Nurnberg, G. *et al.* Refinement of the MYP3 locus on human chromosome 12 in a German family with Mendelian autosomal dominant high-grade myopia by SNP array mapping. *Int. J. Mol. Med.* **21**, 429–438 (2008).
- Shi, Y. *et al.* Genetic variants at 13q12.12 are associated with high myopia in the Han Chinese population. *Am. J. Hum. Genet.* **88**, 805–813. <https://doi.org/10.1016/j.ajhg.2011.04.022> (2011).
- Chiang, S. Y. *et al.* Proteomic analysis and identification of aqueous humor proteins with a pathophysiological role in diabetic retinopathy. *J. Proteomics* **75**, 2950–2959. <https://doi.org/10.1016/j.jprot.2011.12.006> (2012).
- Sharma, S. *et al.* Proteomic alterations in aqueous humor from patients with primary open angle glaucoma. *Invest. Ophthalmol. Vis. Sci.* **59**, 2635–2643. <https://doi.org/10.1167/iovs.17-23434> (2018).
- Su, S. *et al.* Differential proteomic analyses of cataracts from rat models of type 1 and 2 diabetes. *Invest. Ophthalmol. Vis. Sci.* **55**, 7848–7861. <https://doi.org/10.1167/iovs.14-15175> (2014).
- Wang, L. M. *et al.* Proteomic analysis of aqueous humor in acute primary angle-closure glaucoma. *Zhonghua Yan Ke Za Zhi* **55**, 687–694. <https://doi.org/10.3760/cma.j.issn.0412-4081.2019.09.011> (2019).
- Duan, X. *et al.* Proteomic analysis of aqueous humor from patients with myopia. *Mol. Vis.* **14**, 370–377 (2008).
- Yao, J. *et al.* Proteomic analysis of the aqueous humor in patients with wet age-related macular degeneration. *Proteomics Clin. Appl.* **7**, 550–560. <https://doi.org/10.1002/prca.201200012> (2013).
- Kanehisa, M., Sato, Y., Kawashima, M., Furumichi, M. & Tanabe, M. KEGG as a reference resource for gene and protein annotation. *Nucleic Acids Res.* **44**, D457–462. <https://doi.org/10.1093/nar/gkv1070> (2016).
- Kanehisa, M. & Goto, S. KEGG: kyoto encyclopedia of genes and genomes. *Nucleic Acids Res.* **28**, 27–30. <https://doi.org/10.1093/nar/28.1.27> (2000).
- Riddell, N. & Crewther, S. G. Novel evidence for complement system activation in chick myopia and hyperopia models: a meta-analysis of transcriptome datasets. *Sci. Rep.* **7**, 9719. <https://doi.org/10.1038/s41598-017-10277-2> (2017).
- Gentle, A., Liu, Y., Martin, J. E., Conti, G. L. & McBrien, N. A. Collagen gene expression and the altered accumulation of scleral collagen during the development of high myopia. *J. Biol. Chem.* **278**, 16587–16594. <https://doi.org/10.1074/jbc.M300970200> (2003).
- Fukai, N. *et al.* Lack of collagen XVIII/endostatin results in eye abnormalities. *EMBO J.* **21**, 1535–1544. <https://doi.org/10.1093/emboj/21.7.1535> (2002).
- Hay, E. D. Extracellular matrix, cell skeletons, and embryonic development. *Am. J. Med. Genet.* **34**, 14–29. <https://doi.org/10.1002/ajmg.1320340107> (1989).
- Sieglwart, J. T. Jr. & Norton, T. T. Selective regulation of MMP and TIMP mRNA levels in tree shrew sclera during minus lens compensation and recovery. *Invest. Ophthalmol. Vis. Sci.* **46**, 3484–3492. <https://doi.org/10.1167/iovs.05-0194> (2005).
- Xiang, M. *et al.* Identification of proteins in the aqueous humor associated with cataract development using iTRAQ methodology. *Mol. Med. Rep.* **15**, 3111–3120. <https://doi.org/10.3892/mmr.2017.6345> (2017).
- Gao, T. T., Long, Q. & Yang, X. Complement factors C1q, C3 and C5b–9 in the posterior sclera of guinea pigs with negative lens-defocused myopia. *Int. J. Ophthalmol.* **8**, 675–680. <https://doi.org/10.3980/j.issn.2222-3959.2015.04.06> (2015).
- Rossignol, P. *et al.* Protease nexin-1 inhibits plasminogen activation-induced apoptosis of adherent cells. *J. Biol. Chem.* **279**, 10346–10356. <https://doi.org/10.1074/jbc.M310964200> (2004).
- Mignatti, P. & Rifkin, D. B. Biology and biochemistry of proteinases in tumor invasion. *Physiol. Rev.* **73**, 161–195. <https://doi.org/10.1152/physrev.1993.73.1.161> (1993).
- Khokha, R., Martin, D. C. & Fata, J. E. Utilization of transgenic mice in the study of matrix degrading proteinases and their inhibitors. *Cancer Metastasis Rev.* **14**, 97–111. <https://doi.org/10.1007/bf00665794> (1995).
- Price, J. T., Bonovich, M. T. & Kohn, E. C. The biochemistry of cancer dissemination. *Crit. Rev. Biochem. Mol. Biol.* **32**, 175–253. <https://doi.org/10.3109/10409239709082573> (1997).
- Ny, T., Wahlberg, P. & Brandstrom, I. J. Matrix remodeling in the ovary: regulation and functional role of the plasminogen activator and matrix metalloproteinase systems. *Mol. Cell Endocrinol.* **187**, 29–38. [https://doi.org/10.1016/s0303-7207\(01\)00711-0](https://doi.org/10.1016/s0303-7207(01)00711-0) (2002).
- Kwaan, H. C. From fibrinolysis to the plasminogen-plasmin system and beyond: a remarkable growth of knowledge, with personal observations on the history of fibrinolysis. *Semin. Thromb. Hemost.* **40**, 585–591. <https://doi.org/10.1055/s-0034-1383545> (2014).
- Didiasova, M., Wujak, L., Wygrecka, M. & Zakrzewicz, D. From plasminogen to plasmin: role of plasminogen receptors in human cancer. *Int. J. Mol. Sci.* **15**, 21229–21252. <https://doi.org/10.3390/ijms151121229> (2014).
- Godier, A. & Hunt, B. J. Plasminogen receptors and their role in the pathogenesis of inflammatory, autoimmune and malignant disease. *J. Thromb. Haemost.* **11**, 26–34. <https://doi.org/10.1111/jth.12064> (2013).
- Zhou, L. X. *et al.* The relationship between scleral staphyloma and choroidal thinning in highly myopic eyes: the Beijing Eye Study. *Sci. Rep.* **7**, 9825. <https://doi.org/10.1038/s41598-017-10660-z> (2017).
- Curtin, B. J. The myopias, basic science and clinical management. *Optom. Vis. Sci.* **64**(1), 132 (1987).
- Sommer, A. & Tielsch, J. M. Risk factors for open-angle glaucoma: the Barbados Eye Study. *Arch. Ophthalmol.* **114**, 235. <https://doi.org/10.1001/archophth.1996.01100130229029> (1996).
- Chihara, E. *et al.* Severe myopia as a risk factor for progressive visual field loss in primary open-angle glaucoma. *Ophthalmologica* **211**, 66–71. <https://doi.org/10.1159/000310760> (1997).
- Mitchell, P., Hourihan, F., Sandbach, J. & Wang, J. J. The relationship between glaucoma and myopia: the Blue Mountains Eye Study. *Ophthalmology* **106**, 2010–2015. [https://doi.org/10.1016/s0161-6420\(99\)90416-5](https://doi.org/10.1016/s0161-6420(99)90416-5) (1999).
- Jonas, J. B., Martus, P. & Budde, W. M. Anisometropia and degree of optic nerve damage in chronic open-angle glaucoma. *Am. J. Ophthalmol.* **134**, 547–551. [https://doi.org/10.1016/s0002-9394\(02\)01644-6](https://doi.org/10.1016/s0002-9394(02)01644-6) (2002).
- Wong, T. Y., Klein, B. E., Klein, R., Knudtson, M. & Lee, K. E. Refractive errors, intraocular pressure, and glaucoma in a white population. *Ophthalmology* **110**, 211–217. [https://doi.org/10.1016/s0161-6420\(02\)01260-5](https://doi.org/10.1016/s0161-6420(02)01260-5) (2003).
- Xu, L., Wang, Y., Wang, S., Wang, Y. & Jonas, J. B. High myopia and glaucoma susceptibility the Beijing Eye Study. *Ophthalmology* **114**, 216–220. <https://doi.org/10.1016/j.ophtha.2006.06.050> (2007).
- Kuzin, A. A. *et al.* Ocular biometry and open-angle glaucoma: the Los Angeles Latino Eye Study. *Ophthalmology* **117**, 1713–1719. <https://doi.org/10.1016/j.ophtha.2010.01.035> (2010).
- Nagaoka, N. *et al.* Glaucomatous-type optic discs in high myopia. *PLoS ONE* **10**, e0138825. <https://doi.org/10.1371/journal.pone.0138825> (2015).
- Suzuki, Y. *et al.* Risk factors for open-angle glaucoma in a Japanese population: the Tajimi Study. *Ophthalmology* **113**, 1613–1617. <https://doi.org/10.1016/j.ophtha.2006.03.059> (2006).
- Kim, M. J., Kim, M. J., Kim, H. S., Jeoung, J. W. & Park, K. H. Risk factors for open-angle glaucoma with normal baseline intraocular pressure in a young population: the Korea National Health and Nutrition Examination Survey. *Clin. Exp. Ophthalmol.* **42**, 825–832. <https://doi.org/10.1111/ceo.12347> (2014).

40. Morita, H., Funata, M. & Tokoro, T. A clinical study of the development of posterior vitreous detachment in high myopia. *Retina* **15**, 117–124. <https://doi.org/10.1097/00006982-199515020-00005> (1995).
41. Liu, Y. C. *et al.* Eyeball structure changes in high myopic patients and their significance for forensic assessment. *Fa Yi Xue Za Zhi* **24**, 356–360 (2008).
42. Harocopos, G. J. *et al.* Importance of vitreous liquefaction in age-related cataract. *Invest. Ophthalmol. Vis. Sci.* **45**, 77–85. <https://doi.org/10.1167/iovs.03-0820> (2004).
43. Filas, B. A., Shui, Y. B. & Beebe, D. C. Computational model for oxygen transport and consumption in human vitreous. *Invest. Ophthalmol. Vis. Sci.* **54**, 6549–6559. <https://doi.org/10.1167/iovs.13-12609> (2013).
44. Mehdizadeh, M. & Ashraf, H. Prevalence of cataract type in relation to axial length in subjects with high myopia and emmetropia in an Indian population. *Am. J. Ophthalmol.* **146**, 329–330. <https://doi.org/10.1016/j.ajo.2008.04.004> (2008).
45. Praveen, M. R. *et al.* A study to explore the risk factors for the early onset of cataract in India. *Eye* **24**, 686–694. <https://doi.org/10.1038/eye.2009.137> (2010).

Acknowledgements

The authors thank Jing Sun, Xianfeng Shao, Yan Zhang, Yahong Li, Yaoling Li, Yongtao Li, Lujie Zhang and Qing Wang for important clinical and scientific suggestions. No conflicting relationship exists for any author. No honorarium, grant, or other forms of payment was given to anyone to produce the manuscript. Each author listed on the manuscript has seen and approved the submission of this version of the manuscript and takes full responsibility for the manuscript.

Author contributions

Involved in the study concept and design (J.S., Y.Z.); data collection (K.W., X.S., J.S.); analysis of data (K.W., X.S., Y.L., Y.L., Y.L., Q.W., R.S., L.Z., Y.C.); drafting of the manuscript (K.W., X.S.); critical revision of the manuscript (J.S., Y.Z.); statistical expertise (J.S., X.S., Y.L., Y.L., Y.L., Q.W., R.S., L.Z.); administrative, technical, or material support (J.S.); supervision (J.S., Y.Z.); and approval of the manuscript (J.S., Y.Z., K.W., X.S., Y.L., Y.L., Y.L., Q.W., R.S., L.Z., Y.C.). All authors reviewed the manuscript.

Funding

This work was supported by the talent program of Tianjin medical university eye hospital (Grant Number: YDYYRCXM-B2018-01LC); Tianjin clinical key discipline (specialist) construction project under Grant TJLC-ZDXKM004 and Tianjin clinical key discipline (specialist) construction project under Grant TJLCZDXKQ009.

Competing interests

The authors declare no competing interests.

Additional information

Supplementary Information The online version contains supplementary material available at <https://doi.org/10.1038/s41598-021-88220-9>.

Correspondence and requests for materials should be addressed to J.S. or Y.Z.

Reprints and permissions information is available at www.nature.com/reprints.

Publisher's note Springer Nature remains neutral with regard to jurisdictional claims in published maps and institutional affiliations.



Open Access This article is licensed under a Creative Commons Attribution 4.0 International License, which permits use, sharing, adaptation, distribution and reproduction in any medium or format, as long as you give appropriate credit to the original author(s) and the source, provide a link to the Creative Commons licence, and indicate if changes were made. The images or other third party material in this article are included in the article's Creative Commons licence, unless indicated otherwise in a credit line to the material. If material is not included in the article's Creative Commons licence and your intended use is not permitted by statutory regulation or exceeds the permitted use, you will need to obtain permission directly from the copyright holder. To view a copy of this licence, visit <http://creativecommons.org/licenses/by/4.0/>.

© The Author(s) 2021